Archives of Civil and Mechanical Engineering, Volume 22, Issue 1, February 2022, Article number 44
DOI:10.1007/s43452-021-00356-7

# Comparative analysis of cold and warm rolling on tensile properties and microstructure of additive manufactured Inconel 718

Tao Zhang, Huigui Li, Hai Gong, Yunxin Wu, Abdulrahaman Shuaibu Ahmad, Xin Chen & Xiaoyong Zhang

**Abstract:** Despite the high efficiency and low cost of wire + arc additive manufacture (WAAM), the epitaxial grown columnar dendrites of WAAM deposited Inconel 718 cause inferior properties and severe anisotropy compared to the wrought components. Fundamental studies on the influence of one-pass cold and warm rolling on hardness and microstructure were investigated. Then the interpass cold and warm rolling on tensile properties were also analyzed. The results show that the one-pass rolling increases the hardness and displays a heterogeneous hardness distribution compared to the as-deposited material, and the warm rolling exhibits a larger and deeper strain compared to cold rolling. The columnar dendrites gradually change to cell dendrites under the rolling process and then change to equiaxed grains with the subsequent new layer deposition. The average grain size is 16.8 μm and 23.5 μm for the warm and cold rolling, respectively. The strongly textured columnar dendrites with preferred <001> orientation transform to equiaxed grains with random orientation after rolling process. The grain refinement contributes to the dispersive distributed strengthening phases and the increase in its fraction with heat treatment. The as-deposited samples show superior tensile properties compared to the cast material but inferior compared to the wrought components, while the warm-rolled samples show superior tensile properties to wrought material. Isotropic tensile properties are obtained in warm rolling compared to cold rolling. The rolling process and heat treatment both decrease the elongation and lead to a transgranular ductile fracture mode. Finally, the rolling induced strengthening mechanism was discussed.

**Key words**: Wire + arc additive manufacture; cold and warm rolling; microstructure; tensile properties; strengthening mechanism

## 1 Introduction

Inconel 718 (IN-718) is a precipitation strengthened alloy by the heat treatment [1]. It is widely used in the manufacture of turbine components, discs, blades and cartridge receivers of aero-engine, exhaust nozzle and rocket motor due to its high strength and ductility, good corrosion resistance, as well as weldability under 650℃ [2-3]. To improve its overall performance, numerous elements were added to this alloy, thus generating different kinds of secondary phases. The IN-718 alloy consists of the γ austenitic matrix with face centered cubic (Fcc) A1 structure, the γ′-$Ni_3$(Al, Ti) phase with Fcc $L1_2$ structure, the γ″-$Ni_3$Nb phase with body centered tetragonal (Bct) DO22 structure, the δ-$Ni_3$Nb phase with orthorhombic DOa structure, the Laves-(Ni, Cr, Fe)$_2$(Nb, Mo, Ti) phase with hexagonal crystal structure and the MX carbides ((Nb, Ti) (C, N)) with Fcc $B_1$ structure [4]. The γ′ and γ″ phase are the main strengthening phases of the IN-718.

The additive manufacturing process has great potential for the manufacturing of complex components due to its flexibility and material utilization, high efficiency, as well as short manufacturing cycle [5-6]. Cao et al. [7] studied the microstructure and precipitation in solution-heat-treated and double-aging-made IN-718 in selective laser melting process by scanning and transmission electron microscopy. There is coarser acicular γ″ and plate-like δ phases precipitated at grain boundaries and also within the interior of the austenite matrix. The morphology, distribution, and crystallography of these precipitates, as well as their formation mechanisms were analyzed and discussed. Material structure and defects created during additive manufacturing contribute to the wide range of mechanical properties of these parts, thus limiting their use for critical applications. Wire + arc additive manufacture (WAAM) is beneficial for the manufacturing of metal components with large sizes because of its low cost and high deposition rate [8-10]. The metal wire is melted by an electric arc and the components can be deposited layer-by-layer based on its 3D model. There have been few studies focusing on WAAM deposition of

Published by Springer. This is the Author Accepted Manuscript issued with: Creative Commons Attribution Non-Commercial No Derivatives License (CC:BY:NC:ND 4.0).
The final published version (version of record) is available online at DOI:10.1007/s43452-021-00356-7. Please refer to any applicable publisher terms of use.

IN-718. Clark et al. [11] studied the characteristic of single and multiple-layer depositions, as well as the microstructure of the deposited IN-718 alloy in the metal inert gas (MIG) process. Asala et al. [12] found a softened zone of about 2 mm wide at the as-deposited metal's heat affected zone of the deposited IN-718 due to its lowest volume fraction of strengthening precipitates in tungsten inert gas (TIG) process. Furthermore, apart from the MIG and TIG, cold metal transfer (CMT) is a novel form of WAAM technology with high bead quality due to its low heat input. Xu et al. [13] studied the oxidation behavior of IN-718 by the CMT process and observed that the oxides formed on the surface of deposited material had little effect on the tensile properties. Oguntuase et al. [14] investigated the influence of post-deposition heat treatments on the microstructure and mechanical properties of the as-deposited samples. The standard heat treatment degraded the tensile properties and exhibited a profound anisotropic effect at the as-deposited condition, thus a new heat treatment was developed. The directional columnar dendrites of the as-deposited IN-718 result in severe anisotropy. Chen et al. [15] investigated the influence of anisotropy introduced by the WAAM process. The strengths in the longitudinal and transverse direction were higher than that of the normal direction. The anisotropy can be partly modified through quenching and heat treatments by modifying the initial layer-by-layer morphologies. In addition to the tensile properties, Asala et al. [16] comparatively studied the hot corrosion behavior of as-deposited and wrought IN-718 alloy, concluding that the as-deposited material exhibited a significantly lower hot corrosion resistance compared to the wrought condition. The depletion of Nb and Mo in the dendrite core regions decreased the local corrosion resistance and led to the selective hot corrosion attack of these regions.

The residual stress and distortion were the key problems of as-deposited parts. Colegrove et al. [17] applied inter-layer rolling to as-deposited steel. Rolling leads to a reduction in the distortion, surface roughness and residual stress. It also induced grain refinement when the rolled material was reheated during the subsequent deposition pass. The application of rolling may be a key technology for enabling the implementation of WAAM deposition on large-scale structures. Abbaszadeh et al. [18] employed the finite element simulations of the rolling process to investigate the effect of the rolling parameters, particularly rolling load and roller profile radius on the residual stress field as well as plastic strain distribution. The rolling load led to changes in the location, as well as the maximum value and depth of the compressive residual stresses. However, the roller profile radius only changed the maximum value of compressive residual stresses. Tangestani et al. [19] investigated the vertical and pinch rolling effects on residual stress distribution in as-deposited components. The residual stress profile in the vertical rolling process applied on the as-deposited wall can be enhanced by increasing the rolling depth and curvature depth of the roller. However, the residual stress profile in the pinch rolling was sensitive to the rolling direction and more compressive residual stresses can be induced by applying fewer passes of rolling using thicker rollers. Martina et al. [20] evaluated the effect of high-pressure interpass rolling with a flat and a profiled roller, the microstructure changed from large columnar dendrites with several millimeters in the as-deposited sample to equiaxed grains between 56 and 139 μm in size. Gu et al. [21-22] applied cold rolling to aluminum alloy with different rolling loads, the porosity in the as-deposited sample can be eliminated with cold rolling; meanwhile, the mechanical properties can be significantly enhanced by grain refinement and work hardening. Surface waviness was one of the major problems associated with the economic use of the as-deposited components, which causes a significant increase in stress, thus reducing the tensile properties and fatigue life. Dirisu et al. [23] applied cold rolling to as-deposited samples and the

surface waviness reduced from 0.18 to 0.08 mm, which in turn reduces stress concentration, thus reducing crack initiation and propagation, and improving fatigue life. Xu et al. [24] applied interpass cold rolling to plasma deposited IN-718 and alternating bands of finely equiaxed and columnar grains were obtained with the rolling force of 75 kN. The strength of the interpass cold-rolled sample with 75 kN exceeds that of the wrought standard.

However, it was found that the refined microstructure was not uniform, and also, there is a need for special equipment to perform the cold rolling process with the inter-pass cold rolling force of 75 kN. Therefore, warm rolling was considered in this study to increase the deformation depth without the need to increase the rolling force, which can further refine the grains and enhance the uniformity of the microstructural distribution. In this paper, the influence of one-pass cold and warm rolling with flame heating on the hardness and microstructure was comparatively investigated. Then the effect of the new layer deposition on the CET mechanism (columnar dendrites to equiaxed grains transformation) was analyzed. Finally, interpass cold and warm rolling with the same rolling force were performed and their effects on tensile properties, as well as the anisotropy behavior were studied. The rolling-induced strengthening mechanism was revealed based on the microstructural analysis.

## 2 Material and methods

The WAAM deposition system consisted of a power source (Fronius, CMT 4000 advanced), a wire feeder (Fronius, VR 7000) and a torch attached to a 6-axis ABB robot. The rolling system, consisting of a flat roller, a hydraulic cylinder and a CNC system, was integrated into the WAAM deposition system. As shown in Fig.1, the hybrid WAAM deposition and rolling process includes alternating one-layer deposition and one-layer rolling process. The wire diameter of the IN718 is 1.2 mm and its compositions (wt.%) are as follows: 53.15Ni-19.42Cr-5.22Nb+Ta-2.95Mo-0.96Ti-0.47 Al-0.41Cu-0.11Mn-Bal.Fe. The WAAM deposited parameters were described as follows: contact tip-to-work distance (14 mm), wire feed speed (7 m/min), torch travel speed (6 mm/s) and interpass cooling time (3 min). Pure argon was used as the shielding gas and its flow rate was 15 L/min. The diameter and width of the flat roller were 100 mm and 20 mm, respectively. The rolling force with 50 kN was applied and the travel speed of the roller was 5 mm/s. The cold rolling and warm rolling processes were comparatively analyzed in this study. The cold rolling process was applied when the deposited material cooled down to room temperature, while the warm rolling process was achieved by flame heating with a target temperature of 450 ℃. The flame heating was performed immediately after depositing one layer, the infrared camera and thermocouples were used to monitor the temperature variation, as shown in Fig.1 (c).

Firstly, a fundamental study on the cold and warm rolling process was investigated. Two low walls with six layers were deposited and the top surfaces of the walls were cold rolled (CR) and warm rolled (WR); then the $7^{th}$ layer deposition was added to half the length of the rolled surfaces, as shown in Fig.2 (a). The hardness and microstructure of the rolled samples were analyzed. To study the tensile properties of different rolling processes, three high walls with the height of 100 mm to be compared were manufactured: as-deposited (AD), interpass CR and interpass WR. Three horizontal and vertical tensile coupons were cut from the walls, as shown in Fig.2 (b) and Fig.3. The tensile speed was 1 mm/min and a laser extensometer was used for the calculation of elongation.

The standard solution and double aging (SA) heat treatment were applied to the as-deposited, cold and warm rolled samples: solution treated at 970 ℃ and held for 1 h followed by water quenching; aging treated at 720 ℃ and held for 8 h;

furnace cooling to 620 ℃ and held for 8 h followed by air cooling.

The samples were ground and polished for hardness measurement with a load of 1 kg and a holding time of 15 s; then they were etched for microstructure observation using optical microscopy (OM) and scanning electron microscopy (SEM). The energy dispersive spectrometry was used for the quantitative analysis of the precipitates. The grain orientation and the texture were characterized by electron backscatter diffraction (EBSD) analysis.

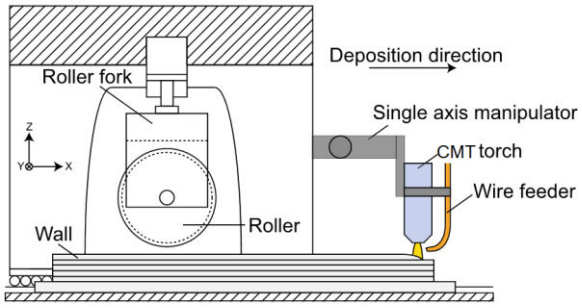


(a) Schematic diagram

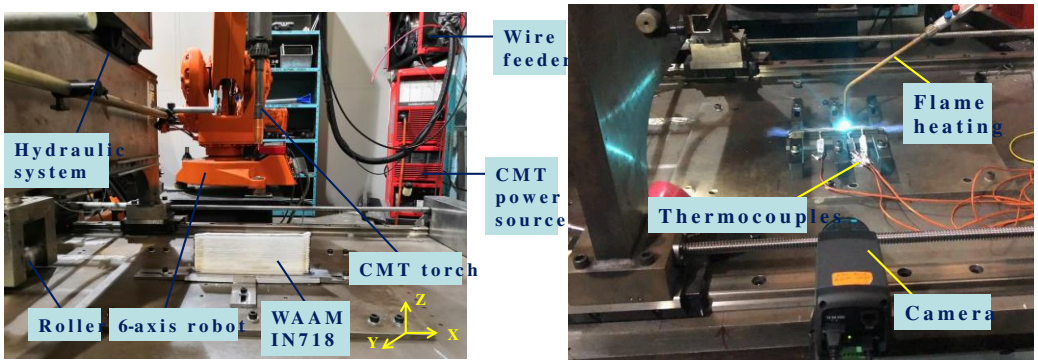


(b) Experimental set up (c) Flame heating

**Fig.1** Hybrid WAAM deposition and rolling process

(a) low wall

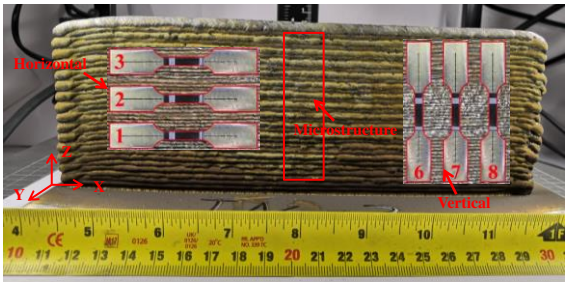


(b) high wall

**Fig.2** IN-718 low walls and high walls after the rolling process

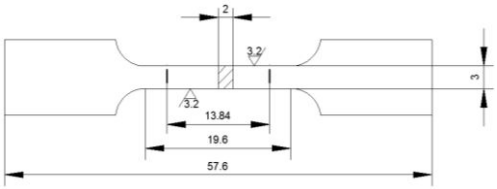


**Fig.3** Dimensions of IN-718 tensile coupon

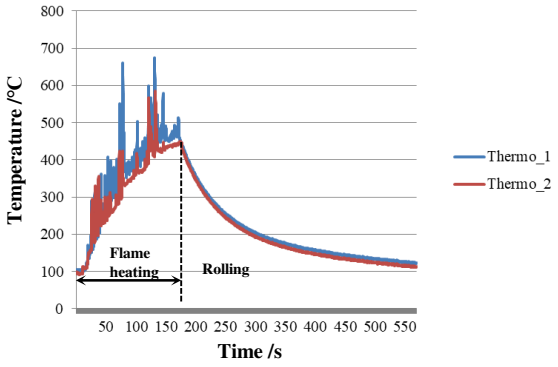


**Fig.4** Temperature variation in the warm rolling process

## 3 Results and discussions

The temperature variation during the warm rolling process is presented in Fig.4. The temperature shows a serrated increase due to the difficulty in precise control of the temperature using flame heating. It takes about 3 mins to attain the target temperature of 450℃, and the warm rolling takes place immediately. Fig.5 shows the sizes of the samples in different rolling processes. The total height decreases from 22.07 mm in as-deposited condition to 19.5 mm and 18.7 mm in the cold and warm rolled condition, respectively. A larger strain was observed in warm-rolled specimen than the cold rolled. The average layer height of the as-deposited sample is 2.82 mm.

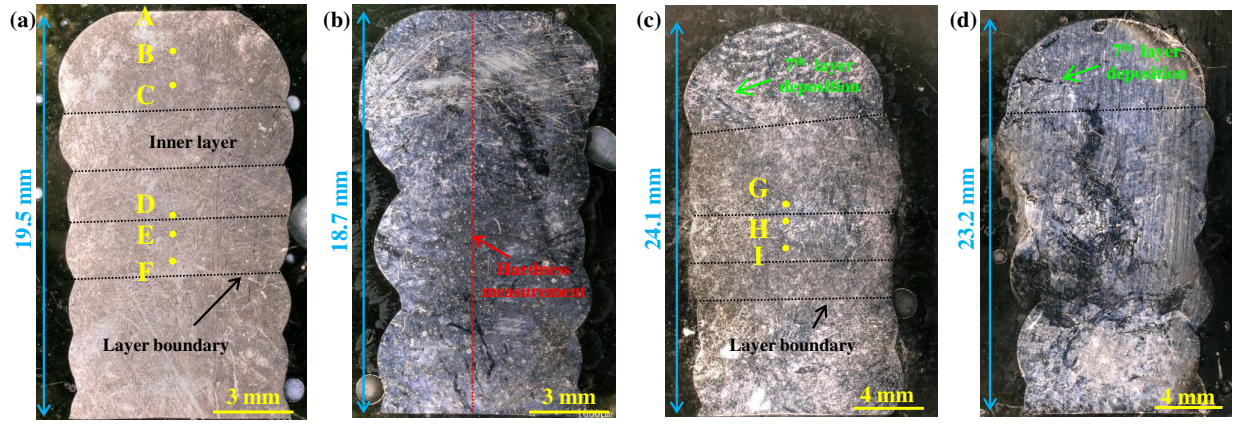


**Fig.5** Schematic diagram of samples with: (a) one-pass cold rolling (CR); (b) one-pass warm rolling; (c) one-pass cold rolling followed by the 7$^{th}$ deposition; (d) one-pass warm rolling followed by the 7$^{th}$ deposition

### 3.1 Hardness

Fig.6 (a) shows the hardness distribution after the one-pass cold and warm rolling processes. An increase in the hardness of the rolled surfaces was observed, which reaches the peak values of 402 HV and 413 HV for the cold and warm rolled, respectively. Then it decreases to a value similar to that of the as-deposited samples. The peak value was observed beneath the rolled surface due to the friction between the roller and the top surface. The hardness curves of the cold and warm rolling primarily intersect at the depth of 6 mm, indicating that the hardened depth induced by the warm rolling is 6 mm. Also, the hardened depth produced due to the cold rolling is 5 mm, there is little variation in the hardness which ranges from 5 mm to 6 mm. In addition, the resulting hardness due to the warm rolling is a bit larger than that of the cold rolling due to its larger and deeper strain. After depositing the new layer on the rolled surfaces, the hardness along the whole thickness decreases for both the cold and warm rolled samples. The heat input from the 7$^{th}$ layer deposition may recover the dislocation density accumulated in the rolling process, resulting in the dynamic softening effect to the rolled samples. It can be seen that the hardness beneath the rolled surface also decreases to the value of the as-deposited condition (about 250 HV), which may be the remelting zone of the new layer deposition. Then, it increases to about 300 HV with increasing depth. The heat input from the new layer deposition will trigger the recrystallization process and the accumulated dislocation density in the rolling process provides the driving force for the growth of recrystallized grains. Recrystallization is essential for grain refinement, which contributes to the hardness increase.

Fig.6 (b) shows the hardness distribution for the interpass as-deposited, interpass cold and warm rolled samples. There is a significant increase in the hardness of the rolled samples compared to that of the as-deposited materials. Nevertheless, the hardness distribution of the interpass rolled samples

is much more uniform than that of the one-pass rolled sample. The repeated cycles of alternating deposition and rolling process during the interpass rolling process may be the reason for the different hardness distribution. There is a dynamic variation of increased dislocation density in the rolling process and decreased dislocation density in the subsequent new layer deposition, thus resulting in a uniform hardness distribution along with the whole thickness. It can be seen that the hardness in the interpass rolled samples is smaller than that of the rolling hardened area in the one-pass rolling process. There is only work hardening in the one-pass rolling process without the new layer deposition on the rolled surface. The hardness in the interpass rolled sample is much larger than that of the unhardened area on the one-pass rolling samples. It may be explained as follows: several cycles of heat input and rolling processes have a significant effect on the hardness increase for its grain refinement strengthening; meanwhile, the repeated heat input provides a temporal aging effect to the previously deposited material.

The hardness of one-pass and interpass rolled samples with standard heat treatment is depicted in Table 1. The heat treatment dramatically increases the hardness for all conditions due to the precipitation strengthening. The samples with one-pass rolling followed by a new layer deposition show the largest value. The warm-rolled samples show a larger value than the specimens treated in the cold-rolled condition. The finer grains in the warm rolled samples contribute to the uniformly distributed precipitates after heat treatment, which will be illustrated in Section 3.3.

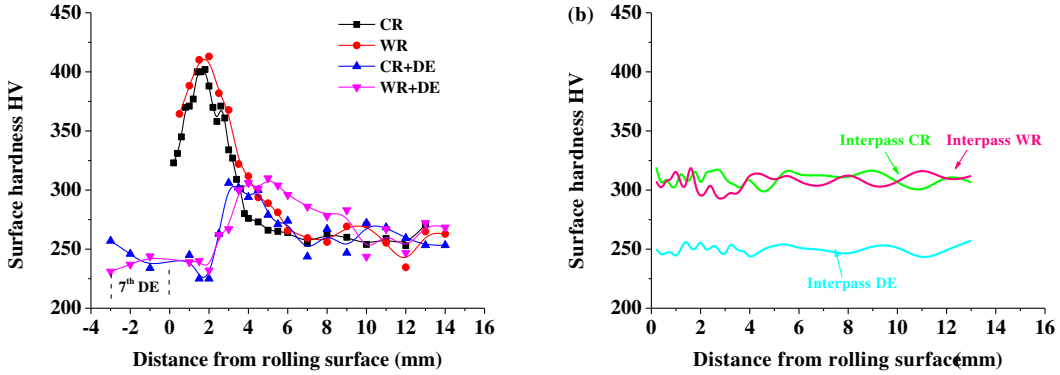


**Fig.6** Hardness distribution without heat treatment of (a) one-pass rolling; (b) interpass rolling.
CR and WR mean one-pass cold and warm rolling, CR+DE means one-pass cold rolling followed by new layer deposition

**Table 1** Hardness variation after heat treatment

| | CR | WR | CR+DE | WR+DE | Interpass DE | Interpass CR | Interpass WR |
|---|---|---|---|---|---|---|---|
| Hardness | 434.4±14.7 | 440.2±23.7 | 443.1±17.3 | 452.8±23 | 406.8±18.6 | 427.1±17.8 | 438.2±20.7 |

### 3.2 Microstructure

The rolling process significantly changes the microstructure of as-deposited IN-718 alloy, as shown in Fig.7. The one-pass rolling process exhibits a heterogeneous distribution of the microstructure. The epitaxial grown columnar dendrites are the typical microstructure of the CMT deposited IN-718 due to its large and directional heat input, as shown in Point C. Its average dendrite arm spacing is about 85 μm while its length can be several millimeters in size through the building direction. Plenty of black Laves phase is precipitated at the inter-dendritic boundaries; that is the micro-segregation during WAAM deposition. The columnar dendrites change to cell dendrites

with the one-pass rolling process in Point A and there is no preferential grown direction of these cell dendrites. Meanwhile, there is an obvious boundary between the columnar and cell dendrites due to the limited hardened depth induced by rolling, as marked with dash lines in Point B.

When depositing a new layer on the rolled surface, three typical zones are generated: the melted zone, transient zone and heat-affected zone. Columnar dendrites appear in the melted zone, which is similar to the microstructure in the as-deposited material. The microstructure due to remelting and fine equiaxed grains both appear in the transient zone with an obvious remelting line, marked with dash line in Point D. The new layer deposition will remelt part of the previously deposited material; meanwhile, its heat input will trigger recrystallization and affect the microstructure beneath the remelting line. As a result, the cell dendrites change into equiaxed grains in the heat affected zone (Point E). Due to the limited hardened depth produced by rolling, there is a mixture of equiaxed grains and columnar dendrites in Point F, indicating that sufficiently accumulated dislocation density in the rolling process is essential for the onset of recrystallization and grain refinement. Both the cold and warm-rolled samples show the heterogeneous distribution of microstructure, ranging from columnar dendrites to the microstructure due to remelting and equiaxed grains. Nevertheless, the average size of the equiaxed grains in the heat affected zone is 23.5 μm and 16.8 μm for the cold and warm rolled samples, respectively. The depth of the zone with equiaxed grains is 0.63 mm and 0.82 mm for the cold and warm rolled samples, respectively (marked with a white arrow in Fig.7). Therefore, finer grains and larger hardened depth can be obtained in the warm rolling in comparison with the cold rolling.

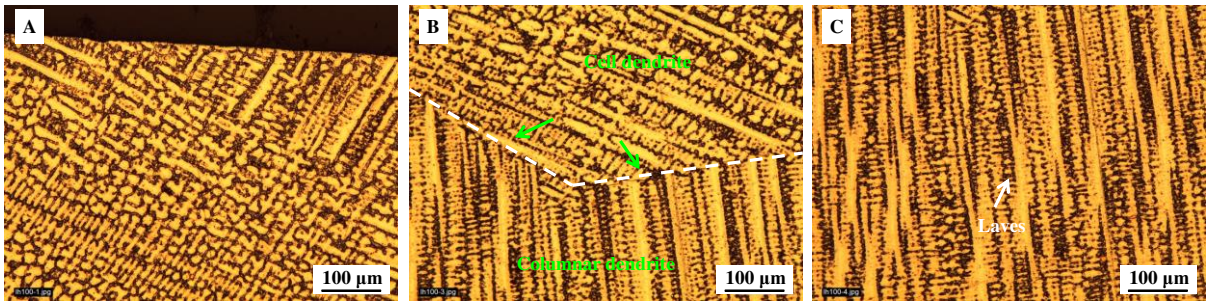

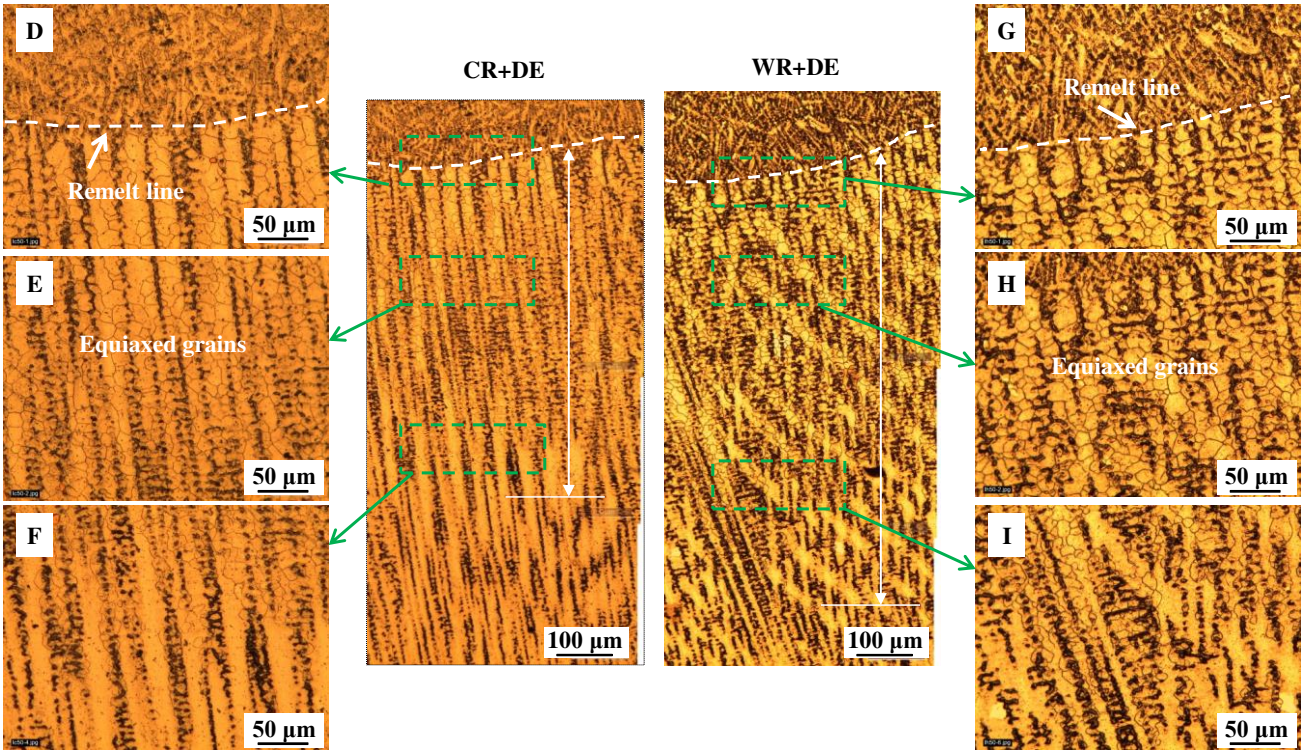


**Fig.7** Microstructure of one-pass rolling process without heat treatment

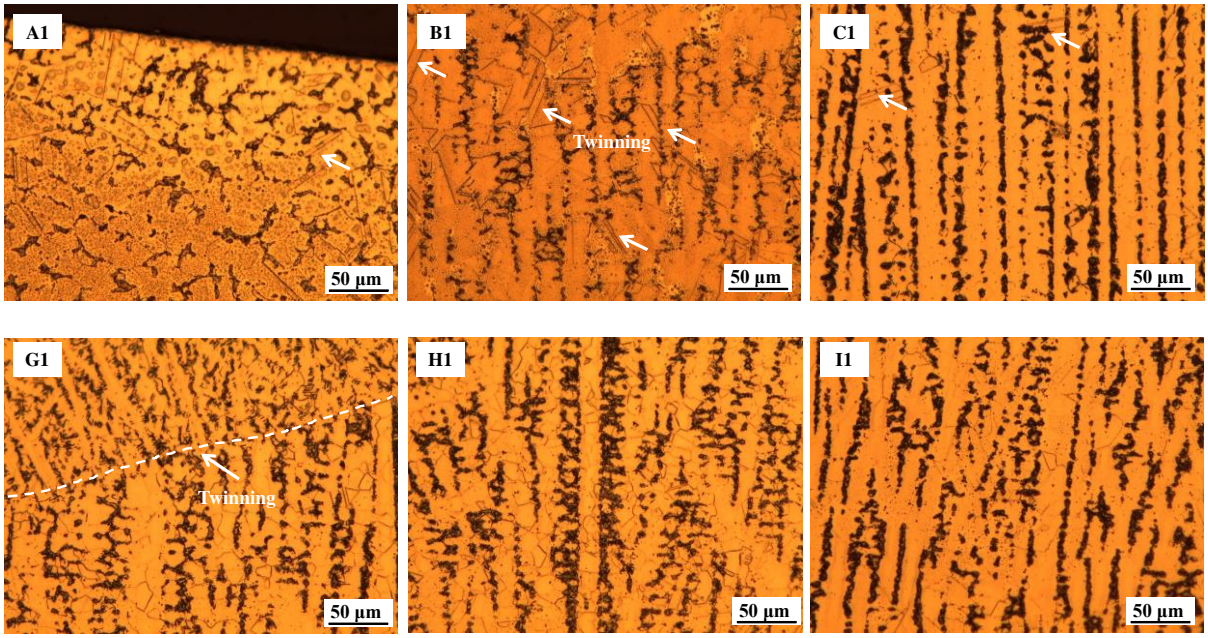


**Fig.8** Microstructure of one-pass rolling process with heat treatment

（Points A1 to I1 correspond to Points A to I in Fig.8 after heat treatment）

Fig.8 shows the microstructure of the one-pass warm rolling after standard heat treatment. It should be noted that Points A1 to I1 corresponds to Points A to I in Fig.7. The microstructure distribution of the one-pass rolling process with standard heat treatment is similar to that without heat treatment. The temperature in the solution and aging process is lower than the recrystallization

temperature of IN-718 [25], as a result, no newly recrystallized equiaxed grains are generated. However, there are a large number of twin crystals in the rolling-hardened zone, especially in the zone with the peak hardness, as shown in Points A1 to C1. After depositing a new layer, the grain boundaries of the equiaxed grains do not significantly vary from the case without heat treatment. The average grain size increases to 21.8 μm, indicating a slight increase in grain growth after heat treatment. Most of the equiaxed grains vary to polygonal grains and even some twin crystals, as shown in Points G1 to I1.

The crystals of the as-deposited material are strongly textured and the grains show a strong <001> preferred growth direction, as shown in Fig.9. The length of the columnar dendrites is several millimeters through the building direction due to the directional heat input from the layer-by-layer WAAM deposition. The strongly textured columnar dendrites change to equiaxed grains with random orientations with cold rolling process. The cold rolling is beneficial to break the columnar dendrites into small sizes; meanwhile, the formation of recrystallized nuclei and its growth due to recrystallization will impede the directional growth of the columnar dendrites. The forged microstructures [26] are composed of large and even grains with an average grain size of 75 μm. Additionally, the forged microstructure shows a high percentage of random high angle grain boundaries. As a result, the intensity for the {100} family of grains oriented along the transverse direction decreases from 7.609 in the as-deposited sample to 3.629 of the cold rolled, which further decreases to 1.698 for the forged material [27]. The wrought material exhibits a texture resembling the rolling texture of an fcc material due to its processing steps.

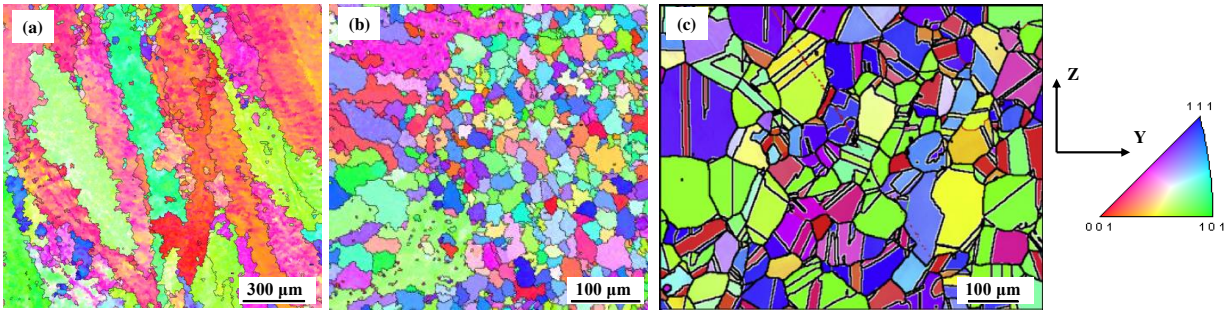


**Fig.9** Grain orientation of: (a) As-deposited; (b) cold-rolled; (c) wrought

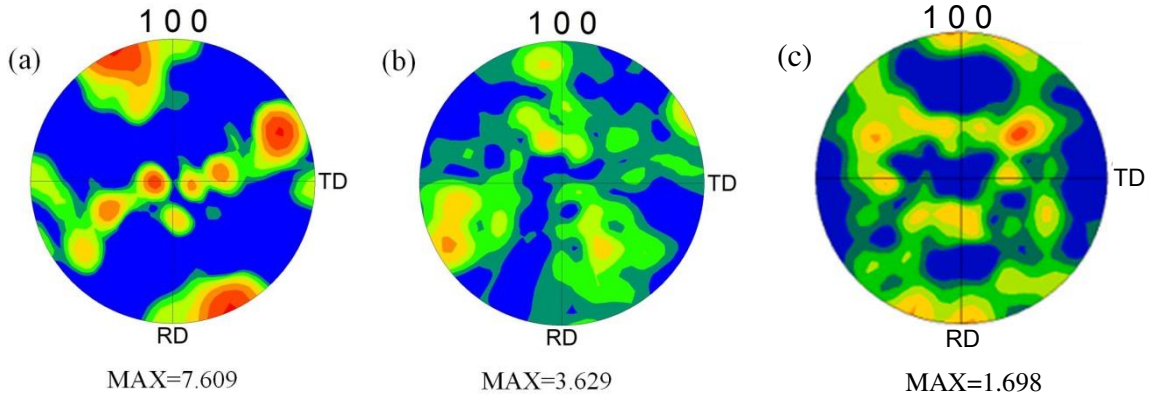


**Fig.10** Pole figures of: (a) As-deposited; (b) cold-rolled; (c) wrought

### 3.3 Precipitation

Fig.11 shows the distribution of precipitates of the as-deposited, cold and warm rolled samples. Discrete islands of Laves phase appear at the interdendritic boundaries, which is similar to the microstructure distribution at Point C shown in Fig.7. Based on the EDS analysis in Fig.12, the white circular particles and needle-like particles around the Laves phases proved to be the MC carbides and δ phase, respectively. The Laves phase is rich in Nb, Cr and Fe; while the MC carbides mainly consist of NbC and TiN. The dissolving temperatures of the Laves phase and MC carbides are over 1080 ℃ and 1340 ℃, respectively [28]. The solution temperature in this study is 970 ℃, which is much lower than the dissolving temperatures of Laves phase and MC carbides. The δ phase is mainly made up of Nb and Ni, it is precipitated at the temperature range of 780 ℃ to 980 ℃, and its peak precipitation temperature is about 900 ℃. Only a small quantity of needle-like δ phase appears in the as-deposited sample as the solution time is so short and sufficient precipitation cannot be achieved. In addition, the aging temperature is 620-720 ℃ and there will be no precipitation of the δ phase in the aging treatment.

For the cold and warm rolled samples, irregular distributed Laves phase and MC carbides are generated and the grain boundary cannot be seen clearly in the rolled zone, as shown in Fig.11 (b) and (c). After depositing a new layer on the rolled surface, the grain boundaries (GB) can be seen clearly, and a large number of small white particles are generated at the GB and grain interiors. This white particle is proved to be the γ" phase, which is the main strengthening phase of the IN-718 alloy. While another strengthening γ' phase of the IN-718 alloy cannot be seen in Fig.11 due to its small size (about several nanometers), which cannot be recognized by SEM.

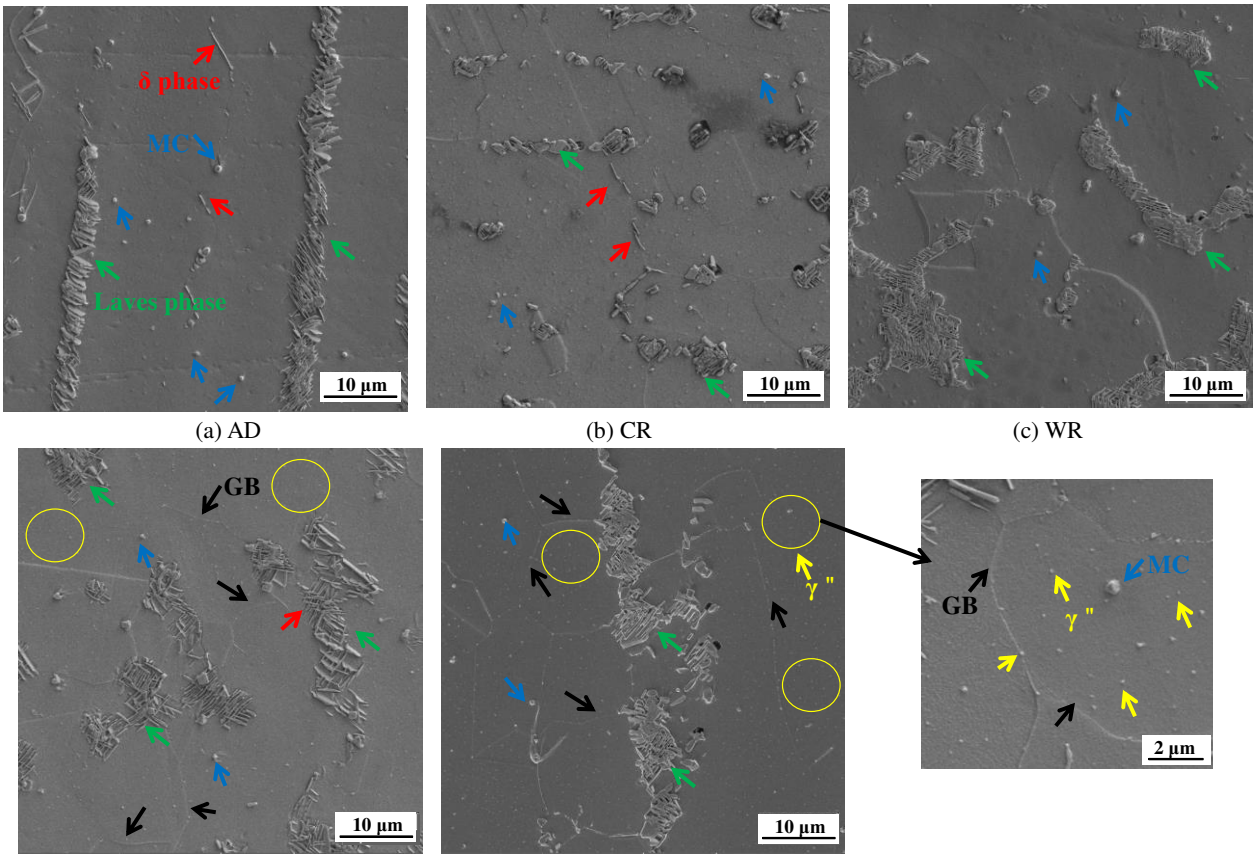


(a) AD (b) CR (c) WR

(d) CR+DE (e) WR+DE

**Fig.11** Precipitation phases in as-deposited, cold and warm rolled IN-718 with heat treatment

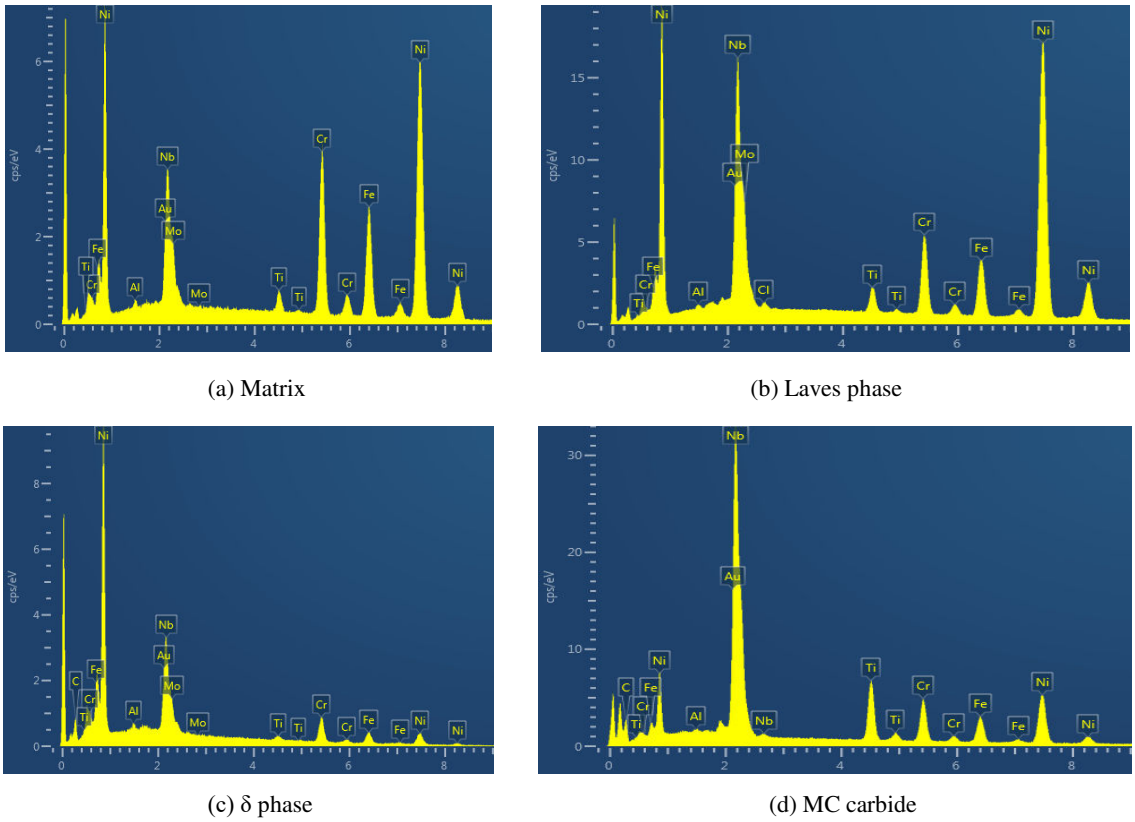


(a) Matrix (b) Laves phase

(c) δ phase (d) MC carbide

**Fig.12** Energy dispersive spectrometry (EDS) analysis of different precipitates

### 3.4 Tensile properties

Fig.13 shows the tensile curves of the as-deposited, cold and warm rolled samples. The rolled samples show higher strength but lower elongation compared to the as-deposited sample without heat treatment. Meanwhile, for the as-deposited sample it can be seen that the difference of elongation at horizontal and vertical direction is quite obvious, and it decreases in rolled conditions. The UTS of the as-deposited sample in the horizontal direction is 840 MPa, which increases to 940 MPa and 972 MPa in warm and cold rolled conditions, respectively. There is a further significant increase of YS from 473 MPa to 666 MPa and 724 MPa for the warm and cold rolled samples, respectively. The elongation in the warm rolled samples slightly increased, while the strength decreased compared to that in cold-rolled. The heat treatment significantly increases the strength and decreases the elongation for all conditions. The horizontal UTS of the as-deposited material increases to 1158 MPa (increased by 37.9%), and the YS increases to 836 MPa (increased by 77.1%) after heat treatment. Also, the horizontal elongation decreases to 16.4% compared to that of the sample before heat treatment (26.3%).

There is a distinct variation in the strength and elongation between the horizontal and vertical direction for the as-deposited sample, which indicates an obvious anisotropy of the tensile properties. It can be observed that the warm rolled samples show minimal anisotropy. To quantitatively describe the anisotropy behavior, an anisotropy coefficient is defined as the ratio of the horizontal value to the vertical value, as shown in Eq.(1). Isotropic tensile properties can be obtained when the anisotropy coefficient equals 1; while the anisotropy increases when the anisotropy coefficient is far away from 1, as shown in Fig.14. The $R$ value of as-deposited samples is far away from 1, especially for the elongation with the value of 0.84. The anisotropy value decreases in the cold rolling process, and it further decreases in the warm

rolling, for instance, the $R$ value of elongation changes to 0.99. Even after heat treatment, the warm-rolled samples show the weakest anisotropy.

$$R=\sigma_H / \sigma_V \quad (1)$$

where $R$ is the anisotropy coefficient, $\sigma_H$ and $\sigma_V$ are the strength or elongation in the horizontal and vertical direction, respectively.

The strength of the as-deposited samples with heat treatment significantly exceeds the cast state (according to AMS5383), while they are far below the wrought material (according to AMS5662). It should be noted that the elongation of the as-deposited samples is much larger than that of the wrought standard even with heat treatment. The strength of the warm-rolled samples is lower without heat treatment compared to the cold-rolled samples, while its strength exceeds that of the cold-rolled samples when heat treatment is performed. The strength and elongation of the warm-rolled samples after heat treatment reaches or exceeds the wrought standard. For the cold-rolled samples, only the strength in the vertical direction is smaller than that of the wrought material due to its anisotropy after heat treatment. The tensile strength of IN-718 varies with different additive manufacturing processes, as shown in Table 3. The LMD (laser metal deposition) and DMD (direct metal deposition) processes show higher strength than the WAAM deposition; and the heat treatment both significantly increase the strengths and decrease the elongation. The powder bed fusion (PBF) process shows the highest strength due to its fastest cooling speed. Nevertheless, the WAAM deposited sample before heat treatment shows the highest ductility due to the slowest cooling rate among these additive manufacturing processes.

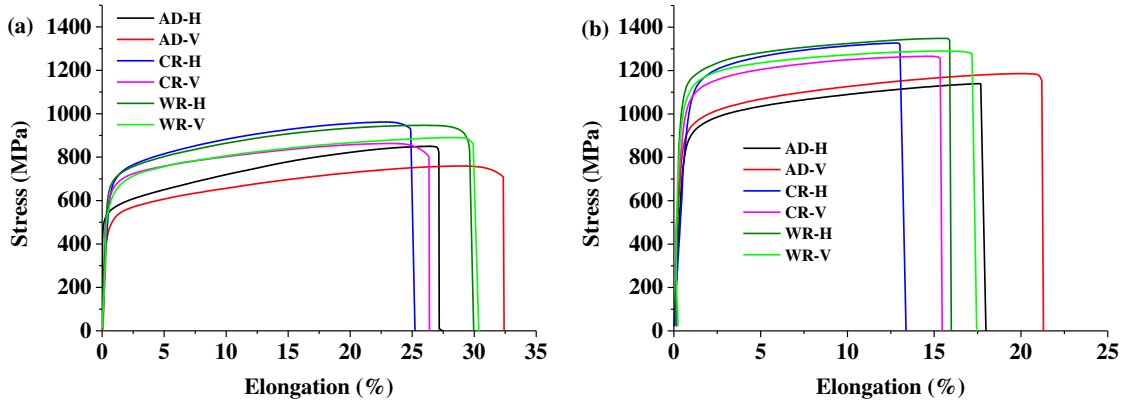


**Fig.13** Tensile curves of IN-718: (a) without heat treatment; (b) with standard heat treatment (H: horizontal, V: vertical)

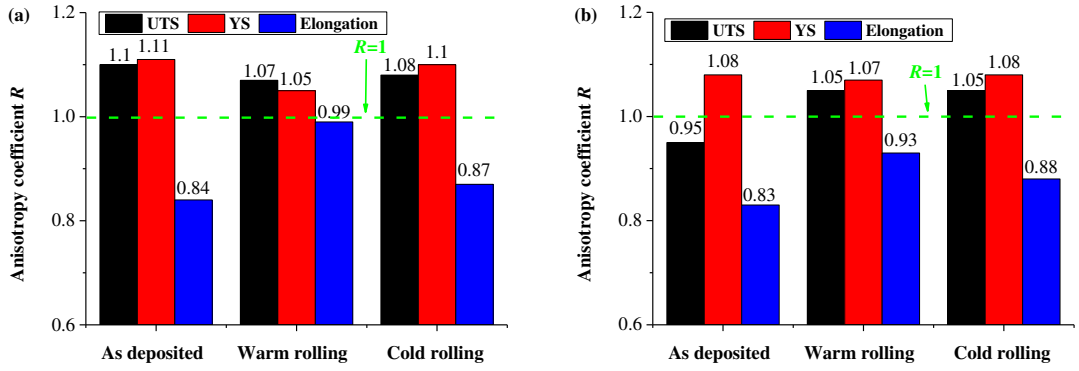


**Fig.14** Anisotropy coefficient of IN-718: (a) without heat treatment; (b) with standard heat treatment

**Table 2** Tensile test results of IN-718 alloy

| | UTS/MPa | | YS/MPa | | Elongation (%) | |
|---|---|---|---|---|---|---|
| | H | V | H | V | H | V |
| AD | 840.7±13.3 | 766.2±6.9 | 472.5±9.5 | 425.9±9.6 | 26.3±1.1 | 31.3±0.8 |
| AD-SA | 1158±18.2 | 1217.3±31 | 836.3±18.8 | 771.9±30.9 | 16.44±1.24 | 19.92±2.89 |
| Interpass WR | 940.1±23.7 | 875±22.6 | 666.3±39.6 | 633.9±32.3 | 30.2±2.8 | 30.4±4.2 |
| Interpass WR-SA | 1341.5±20.5 | 1282.5±20.5 | 1085.5±23.3 | 1011±22.6 | 15.7±1.13 | 16.95±1.2 |
| Interpass CR | 971.7±19 | 896.1±23.3 | 724.3±18.2 | 657.7±15.2 | 24.2±1.8 | 27.8±3.7 |
| Interpass CR-SA | 1330.4±4.3 | 1264.4±2.9 | 1035±9.9 | 960.5±27.7 | 13.75±1.5 | 15.59±0.35 |
| Wrought AMS5662[29] | | 1276 | | 1034 | | 12 |
| Cast AMS5383[30] | | 862 | | 758 | | 5 |

**Table 3** Tensile strength of IN-718 with various additive manufacturing process

| | UTS/MPa | YS/MPa | Elongation (%) |
|---|---|---|---|
| PBF-AD [31] | 1126 | 849 | 22.8 |
| PBF-SA [31] | 1371 | 1084 | 10.1 |
| WAAM-AD [14] | 764 | / | 34.6 |
| WAAM-SA[14] | 1022 | / | 13.2 |
| LMD-AD [32] | 856 | 567 | 34 |
| DMD-AD [33] | 904 | 552 | 16.2 |
| DMD-SA [33] | 1221 | 1007 | 16 |

PBF: powder bed fusion; LMD: laser metal deposition DMD: direct metal deposition; AD: as deposited; SA: standard heat treatment

### 3.5 Fracture morphology

Fig. 15 shows the fracture surfaces of the as-deposited, cold and warm rolled samples during tensile test using SEM. The columnar dendritic pattern with fine dimples before heat treatment changes to an equiaxed pattern with shallow dimples on the as-deposited samples after heat treatment. The main fracture mechanism is the transgranular fracture mode, indicating good ductility of the as-deposited samples. Uniformly distributed dimples with particles inside the dimples are formed on the rolled surfaces (with yellow arrow). Based on the EDS analysis, these particles mainly consist of Laves phase, MC and strengthening phases. These particles may be the preferential positions for the coalescence and propagation of the microvoid, thus leading to fracture during the tensile test. Therefore, the rolled samples display inferior ductility than the as-deposited. The warm rolled samples show deeper and more dispersive distributed dimples, resulting in a higher elongation compared to the cold rolled. The heat treatment dramatically decreases the elongation for all conditions with the appearance of some brittle characteristics, such as the flat surface of the warm-rolled sample and cracks of the cold-rolled sample.

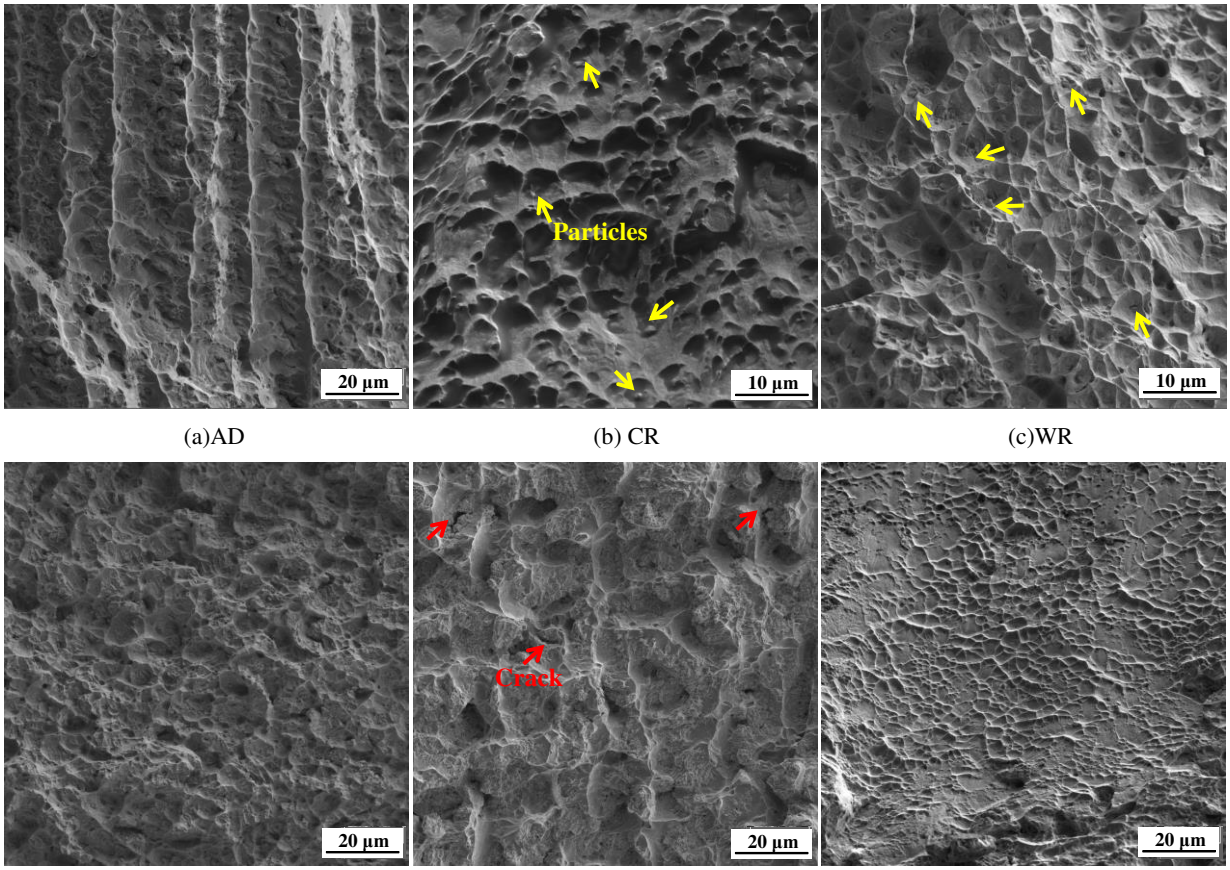


(a)AD (b) CR (c)WR

(d)AD (e) CR (f) WR

**Fig.15** Fracture surfaces of the tensile test without heat treatment (a-c) and with standard heat treatment (d-f)

### 3.6 Rolling induced strengthening mechanism

As discussed in Section 3.4, the as-deposited material with heat treatment shows superior tensile properties to the cast material. WAAM deposition significantly differs from the casting process due to its dynamic heat transfer of moving heat source and the layered material deposition mechanism. The cooling rate in the WAAM deposition is much higher than that in the casting process due to its characteristic of partial melting-solidification. Therefore, the microsegregation is less in WAAM deposition, thus resulting in higher strengths compared to cast material.

The rolling process significantly increases the strength and decreases the elongation. Meanwhile, the anisotropy behavior can also be decreased in the rolling process. The columnar dendrites change to cell dendrites during one-pass rolling and finer equaixed grains can be obtained with new layer deposition, as shown in Fig.8. The accumulated deformation energy during the rolling process and the heat input from the deposition both contribute to the triggering of the recrystallization process. The grain boundary strengthening contributes to the strength increase during the rolling process. According to the Hall-Petch relationship, the strength is inversely proportional to the average grain size. As shown in Fig. 7, the dendrite arm spacing is 85 μm while its length is several millimeters, which results in the large difference between the strength in the horizontal and vertical direction, thus causing severe anisotropy behavior. The equiaxed grains with smaller size in the rolling process increases the strength and decreases the anisotropy.

As discussed in Section 3.1, the hardened depth produced due to the cold rolling is 5 mm, which is a bit larger in the warm rolling due to its larger and deeper strain. Additionally, the thickness

of the overlay layer will affect the distribution of the microstructure, thus changing the mechanical properties. The thickness of the overlay layer is related to the torch travel speed and the heat input, according to Cong's results [34]. It can be seen from Fig.8 that there is a melted zone due to the remelting process with the subsequent deposition. The increased thickness of the overlay layer will increase the depth of the melted zone, thus will increase the inhomogeneity of the distribution of the microstructure. The rolling hardened depth is much larger than the average layer height of the as-deposited sample, which contributes to the formation of equiaxed grains and enhancement of mechanical properties.

After heat treatment, there are many annealing twins for the rolled samples, especially at the rolling-hardened zone, as shown in Fig.9. Annealing twins usually appear in the FCC metal with low stacking fault energy after solution treatment. The grain boundaries of annealing twins can provide the nucleation positions for the newly recrystallized grains [26]. Meanwhile, the dislocation is likely to be tangled at the twin boundaries. The increase in the twin boundaries increases the strength of the material after heat treatment. As shown in Fig.11, many strengthening γ" phases are generated both at the grain boundaries and grain interiors. Finer grains of the rolling process increase the number of grain boundaries and volume fraction of the strengthening phases, thus leading to a more dispersive distribution of strengthening phases. Both the strengthening phases and the grain boundaries will impede the dislocation motion, which significantly increases the strengths. Additionally, the volume of the δ phase in the warm rolling is larger than that in the cold rolling process. The effect of the δ phase on the strengths can be explained as follows: Nb is the vital element of the strengthening phases of the IN-718 alloy. The atomic fraction of Nb in the γ" phase, δ phase and Laves phase is 4%, 6~8% and 10~12%, respectively [31]. Laves phase is generated inevitably during the WAAM deposition and it cannot completely be dissolved during the heat treatment. A more precipitated δ phase may deplete the Nb fraction of the matrix and decrease the fraction of the strengthening phases after heat treatment. Therefore, less δ phase in the warm-rolled samples contributes to the higher strength than the cold-rolled samples with heat treatment.

The WAAM deposited samples show inferior tensile properties than the wrought material; while the interpass warm rolled samples reach or exceed the wrought standard. Several thermal cycles of hot deformation and heat treatments are applied to wrought material, where finer equiaxed grains and dispersive distributed strengthening precipitates can be obtained. Meanwhile, the detrimental Laves phase can be completely dissolved at high temperatures in the homogenization treatment, and the grain growth can be controlled under several cycles of deformation plus heat treatments. Therefore, excellent and isotropic mechanical properties can be obtained in wrought material. Finer equiaxed grains with a certain depth beneath the remelting microstructure can be obtained due to the recrystallization mechanism in the rolling process. The interpass warm rolling process provides the plastic deformation and grain refinement equivalent to the wrought material, thus its strength and elongation are larger than that of the wrought standard. This study provides guidance for the manufacturing of the near-net-shape components of superalloys and only small machining allowance is needed for the final components.

# 4 Conclusions

The effects of one-pass and interpass rolling on the hardness, microstructure and tensile properties of as-deposited IN-718 were investigated.

(1) One-pass rolling process causes a heterogeneous hardness distribution while the interpass rolling gives a much more uniform

distribution. The warm rolling induces a bit larger and deeper hardness than the cold rolling.

(2) The columnar dendrites change to cell dendrites during one-pass rolling and then changes to equiaxed grains of 23.5 μm and 16.8 μm in cold and warm rolling process with new layer deposition. The strongest intensity for the {100} family of grains oriented along the transverse direction is 7.609 of as-deposited samples, which decreases to 3.629 after rolling.

(3) The warm rolled samples show superior tensile properties compared to as-deposited and cold-rolled samples, and it reaches or exceeds the wrought standard. More dispersive distributed strengthening phases and finer grains both contribute to the strengths increase and isotropic tensile properties.

(4) The rolling induced strengthening mechanism mainly consists of work hardening, grain boundary strengthening and precipitation strengthening. The grain boundary also affects the dispersive distributed strengthening phases, thus improving the strength increase in the warm rolling process.

(5) The warm rolling process can improve the tensile properties and enhance the isotropic behavior compared to the cold rolling process.

### Declaration of Competing Interest

The authors declare that they have no known competing financial interests or personal relationships that could have appeared to influence the work reported in this paper.


### Acknowledgements

The authors wish to acknowledge the financial support from the State Key Laboratory for High Performance Complex Manufacturing, Central South University (ZZYJKT2021-05).


## Reference


1. Yang X, Wang B, Jiang W, Shen S, Wang J. The superplasticity improvement of Inconel 718 through grain refinement by large reduction cold rolling and two-stage annealing. Mater Sci Eng A 2021; 823: 141713.
2. Shen XH, Gong XH, Wang BL, He JQ, Xu CH, Su GS. Surface properties enhancement of Inconel 718 alloy by ultrasonic roller burnishing coupled with heat treatment. Arch Civ Mech Eng 2021; 21:1-17.
3. Cui XL, Yuan S. Analysis of thickness variation and stress state in hydroforming of complex T-shaped tubular part of nickel-based superalloy. Arch Civ Mech Eng 2021; 21:111.
4. Kuo YL, Horikawa S, Kakehi K. The effect of interdendritic δ phase on the mechanical properties of alloy 718 built up by additive manufacturing, Mater. Design. 2017; 116: 411-418.
5. Dang J, Cai X, Yu D, An Q, Ming W, Chen M. Effect of material microstructure on tool wear behavior during machining additively manufactured Ti6Al4V. Arch Civ Mech Eng 2020; 20:1-15.
6. Song B, Yu T, Jiang X , Xi W, Lin X. The relationship between convection mechanism and solidification structure of iron-based molten pool by laser direct deposition. Int J Mech Sci 2019; 165:105207.
7. Cao GH, Sun TY, Wang CH, Li X, Liu M, Zhang ZX, Hu PF, Russell AM, Schneider R, Gerthsen D. Investigations of γ′, γ″ and δ precipitates in heat-treated Inconel 718 alloy fabricated by selective laser melting. Mater Charact 2018; 136:398-406.
8. Manurung Y, Prajadhiana KP, Adenan MS, Awiszus B, Haelsig A. Analysis of material property models on WAAM distortion using nonlinear numerical computation and experimental verification with P-GMAW. Arch Civ Mech Eng 2021; 21: 32.
9. Wu B, Pan Z, Ding D, Cuiuri D, Li H, Xu J, Norrish J. A review of the wire arc additive manufacturing of metals: properties, defects and quality improvement. J Manuf Process 2018; 35: 127-139.
10. Williams S, Martina F, Addison A, Ding J, Pardal G, Colegrove P. Wire + arc additive manufacturing. Mater Sci Tech-Lond 2016; 7: 641-647.
11. Clark D, Bache MR, Whittaker MT. Shaped metal deposition of a nickel alloy for aero engine applications. J Mater Process Tech 2008; 203: 439-448.
12. Asala G, Khan AK, Andersson J, Ojo OA. Microstructural analyses of ATI 718Plus® produced by wire-ARC additive manufacturing process. Metall Mater Trans A 2017; 48: 4211-4228.
13. Xu X, Ding J, Ganguly S, Williams S. Investigation of process factors affecting mechanical properties of INCONEL

718 superalloy in wire+ arc additive manufacture process. J Mater Process Tech 2019; 265: 201-209.

14. Oguntuase O, Ojo OA, Beddoes J. Influence of post-deposition heat treatments on the microstructure and mechanical properties of wire–arc additively manufactured ATI 718Plus. Metall Mater Trans A 2020; 51: 1846-1859.
15. Chen C, Pan Z, Ding D, Yuan L, Li H. The influence of post-production heat treatment on the multi-directional properties of nickel-aluminum bronze alloy fabricated using wire-arc additive manufacturing process. Addit Manuf 2018; 23: 411-421.
16. Asala G, Andersson J, Ojo OA. Hot corrosion behaviour of wire-arc additive manufactured Ni-based superalloy ATI 718Plus®. Corros Sci 2019; 158: 108086.
17. Colegrove PA, Coules HE, Fairman J, Martina F, Kashoob T, Mamash H, Cozzolino LD. Microstructure and residual stress improvement in wire and arc additively manufactured parts through high-pressure rolling. J Mater Process Tech 2013; 213: 1782-1791.
18. Abbaszadeh M, Honnige JR, Martina F, Neto L, Kashaev N, Colegrove P, Williams S, Klusemann B. Numerical investigation of the effect of rolling on the localized stress and strain induction for wire + arc additive manufactured structures. J Mater Eng Perform 2019; 28: 4931-4942.
19. Tangestani R, Farrahi GH, Shishegar M, Aghchehkandi BP, Mehmanparast A. Effects of vertical and pinch rolling on residual stress distributions in wire and arc additively manufactured components. J Mater Eng Perform 2020; 29: 2073–2084.
20. Martina F, Colegrove PA, Williams SW, Meyer J. Microstructure of interpass rolled wire + arc additive manufacturing Ti-6Al-4V components. Metall Mater Trans A 2015; 46: 6103-6118.
21. Gu J, Ding J, Williams SW, Gu H, Ma P, Zhai Y. The effect of inter-layer cold working and post-deposition heat treatment on porosity in additively manufactured aluminum alloys. J Mater Process Tech 2016; 230: 26-34.
22. Gu J, Wang X, Bai J, Ding J, Williams SW, Zhai Y, Kun L. Deformation microstructures and strengthening mechanisms for the wire+arc additively manufactured Al-Mg4.5Mn alloy with inter-layer rolling. Mater Sci Eng A 2018; 712: 292-301.
23. Dirisu P, Supriyo G, Martina F, Xu X, Williams S. Wire plus arc additive manufactured functional steel surfaces enhanced by rolling. Int J Fatigue 2020; 130: 105237.
24. Xu X, Ganguly S, Ding J, Seow C, Williams S. Enhancing mechanical properties of wire+ arc additively manufactured INCONEL 718 superalloy through in-process thermomechanical processing. Mater Design 2018; 160: 1042-1051.
25. Lin YC, He DG, Chen MS. EBSD analysis of evolution of dynamic recrystallization grains and delta phase in a nickel-based superalloy during hot compressive deformation. Mater Design 2016; 97: 13-24.
26. Chen XM, Lin YC, Wu F. EBSD study of grain growth behavior and annealing twin evolution after full recrystallization in a nickel-based superalloy. J Alloy Compd 2017; 724: 198-207.
27. Varga J, Kingstedt O T. An investigation of the plastic work to heat conversion of wrought and laser powder bed fusion manufactured Inconel 718. Addit Manuf 2021; 46:102179.
28. Seow CE, Coules HE, Wu G, Khan RHU, Williams S. Wire + Arc Additively Manufactured Inconel 718: Effect of post-deposition heat treatments on microstructure and tensile properties. Mater Design 2019183: 108157.
29. SAE. Aerospace, Aerospace Material Specification: AMS 5662. SAE International 2009.
30. SAE. Aerospace, Aerospace Material Specification: AMS 5383. SAE International 2012.
31. Zhang D, Niu W, Cao X, Liu Z. Effect of standard heat treatment on the microstructure and mechanical properties of selective laser melting manufactured Inconel 718 superalloy. Mater Sci Eng A 2015; 644: 32–40.
32. Wang Y, Shi J. Recrystallization behavior and tensile properties of laser metal deposited Inconel 718 upon in-situ ultrasonic impact peening and heat treatment. Mater Sci Eng A 2020; 786: 139434.
33. Qi H, Azer M, Ritter A. Studies of standard heat treatment effects on microstructure and mechanical properties of laser net shape manufactured INCONEL 718. Metall Mater Trans A 2009; 40: 2410-2422.
34. Cong B, Ding J, Williams S. Effect of arc mode in cold metal transfer process on porosity of additively manufactured Al-6.3%Cu alloy. Int J Adv Manuf Tech 2015; 76:1593-1606.

https://dspace.org/

# Comparative analysis of cold and warm rolling on tensile properties and microstructure of additive manufactured Inconel 718

**Zhang, Tao; Li, Huigui; Gong, Hai; Wu, Yunxin; Ahmad, Abdulrahaman Shuaibu ...**

**2022-01-14**
Springer
https://doi.org/10.1007/s43452-021-00356-7
Zhang T, Li H, Gong H, et al., (2022) Comparative analysis of cold and warm rolling on tensile properties and microstructure of additive manufactured Inconel 718. Archives of Civil and Mechanical Engineering, Volume 22, Issue 1, February 2022, Article number 44

Downloaded from a DSpace repository. https://dspace.org/